CrossMark

Estimation of Fracture Toughness of Metallic Materials Using Instrumented Indentation: Critical Indentation Stress and Strain Model

S.-W. Jeon[1] (iD) · K.-W. Lee[2] · J.Y. Kim[1] · W.J. Kim[1] · C.-P. Park[1] · D. Kwon[1]

Abstract We propose a generalized approach based on fracture mechanics and contact mechanics to estimate the fracture toughness in metallic materials from instrumented indentation testing. Models were developed for brittle and ductile fracture. Different criteria were applied to each model to determine the critical fracture point during indentation. For brittle fracture, the critical fracture point was defined in terms of the critical mean pressure; for ductile fracture, the critical fracture point was derived from fracture strain and critical plastic zone size. Each fracture criterion was used to determine the indentation fracture energy corresponding to the fracture energy required for crack extension. The fracture toughness was estimated for various metallic materials using each model and compared with standard fracture toughness tests.

Introduction

Fracture toughness, defined as a material's resistance to crack propagation, is one of the most important aspects of structural integrity. Fracture toughness can be measured using standardized test methods such as those developed by ASTM and BS [1–3]. However, it can be difficult to measure fracture toughness with these methods because they require specific specimen dimensions and complex test procedures to validate the measured values. In addition, standard measurements cannot be applied to small-volume regions (e.g., weld zones, thin films) or to in-service industrial structures because of the requirements of the test procedures and the destructive nature of the tests. Among the alternative test methods available, indentation testing is widely used to evaluate fracture toughness because of the simplicity of the test procedure and specimen preparation. In addition, indentation testing can be applied to small-volume regions and in-service structures because it is localized and nondestructive in nature. The research on indentation fracture toughness has focused primarily on brittle materials such as glass and ceramics because cracking is induced in such materials upon contact with the indenter. Lawn et al. [4] showed that the fracture toughness (K_{IC}) can be determined based on the relation between the crack length and the indentation load using linear elastic fracture mechanics.

However, in ductile materials such as metals, cracking does not occur during indentation. Some researchers [5–8] have attempted to use indentation to estimate the fracture toughness of ductile materials by adopting a criterion for a critical point corresponding to the onset of crack extension. The modified critical strain model [5, 6], the indentation energy to fracture (IEF) model [7] and the critical indentation energy model based on continuum damage mechanics [8] have been proposed for this purpose. In these models [5–8], the stress state similarity beneath an indenter tip and in front of a crack tip is an important theoretical basis that enables estimation of the fracture toughness from indentation tests. Lee et al. [8] analyzed the stress state ahead of the crack tip and beneath the spherical indenter tip using the finite element method; their results showed that the degree of tri-axial stress generated by

✉ S.-W. Jeon
  jeonsw@snu.ac.kr

[1] Department of Materials Science and Engineering, Seoul National University, 1 Gwanak-ro, Gwanak-gu, Seoul 151-744, South Korea

[2] Product Quality Assurance Team, Memory Division, Samsung Electronics, San 16 Banwol-Dong, Hwasung-City, Gyeonggi-Do 445-701, South Korea

indentation with a spherical indenter is similar to that ahead of the crack tip. The plastic deformation zone generated by the tri-axial stress under the indenter is constrained by the surrounding elastic material in much the same way as ahead of a sharp notch. Lee et al. [8] proposed that fracture toughness can be predicted by determining the critical indentation depth corresponding to the crack extension. They assumed that a fracture was initiated when the volume fraction of voids nucleated within the indented material reached a critical fraction. They proposed that this critical void volume fraction can be calculated from the variation in the elastic modulus evaluated by an indentation test. However, this approach is difficult to apply because the elastic modulus during indentation is strongly affected by machine compliance. In addition, the estimated fracture toughness of metals [5–8] has been limited to specific ranges for brittle metallic materials (K_{IC} <10 MPa · m$^{0.5}$) and ductile metallic materials (K_{JC} >250 MPa · m$^{0.5}$).

We propose a generalized approach to estimate the fracture toughness of metallic materials using instrumented indentation testing with a spherical indenter. The concepts of critical fracture stress and critical fracture strain are applied to construct a new fracture toughness model based on the fracture behavior characteristics of metallic materials. In typical fracture phenomena, there are two general types of fracture behavior: brittle fracture and ductile fracture. Brittle fracture occurs with little or no plastic deformation and very little energy absorption and is usually characterized by a flat cleavage fracture surface with little or no ductility. In the initiation of cleavage fracture, the material separates within the crack tip when a critical stress is reached at a material element near the crack tip [9]. The critical stress criterion can be applied to metallic materials showing cleavage fracture, that is, brittle fracture can be initiated when the local stress becomes large enough to drive a crack from the brittle phase [9]. Thus, brittle fracture initiates in a material beneath an indenter when the local stress exceeds a critical value during indentation testing. We define the critical value through stress analysis based on contact mechanics. The model applied to brittle metallic materials, called the critical indentation stress model, is applicable to brittle metallic materials with relatively low fracture toughness (K_{JC} < 100 MPa · m$^{0.5}$) or in the lower shelf region of the ductile-brittle transition curve. In contrast, ductile fracture occurs with large amounts of plastic deformation and is usually characterized by large shear lips and tearing. In locally ductile fracture initiation, the critical strain criterion can be applied to metallic materials with tearing [9], that is, a critical level of crack tip strain causes ductile void nucleation and coalescence [9]. Thus, we assume that the rate of energy release due to ductile fracture is equivalent to the plastic work induced by the strain ahead of the crack tip. We attempt to estimate the plastic work by evaluating the plastic work induced by indentation strain. The model applied to ductile metallic materials, called the critical indentation strain model, is applicable to ductile

metallic materials with relatively large fracture toughness (K_{JC} > 250 MPa · m$^{0.5}$) or in the upper shelf region of the ductile-brittle transition curve.

Theoretical Modeling

Critical Indentation Stress Model

The indentation critical stress model assumes that brittle fracture is initiated in a material beneath an indenter when the local stress exceeds a critical value. To determine this critical value, we analyze the indentation stress field using contact mechanics. When the indenter and the specimen have elastic contact, the stress components in the radial and hoop directions outside the contact circle are given by Hertz's elastic contact theory [10], as in equation (1); Fig. 1 shows a schematic diagram of the stress field according to Hertz's theory.

$$\frac{\sigma_r}{p_m} = -\frac{\sigma_\theta}{p_m} = \frac{(1-2\nu)}{2}\frac{a^2}{r^2} \tag{1}$$

Here, σ_r is the stress in the radial direction, σ_θ is the stress in the hoop direction, p_m is the mean pressure over the contact area, a is the contact radius, ν is Poisson's ratio and r is the radial distance from the center of the contact. The stress component, σ_r, is tensile outside the contact circle, as shown in equation (1), and it induces ring cracks when a critical indentation load is applied to a brittle material, such as a glass or ceramic [11]. The stress reaches its maximum value at the edge of the contact circle, $r = a$. Although initial plastic yielding is initiated at a depth of approximately $0.48a$ beneath the indenter, the elastic solution is valid as long as p_m does not exceed the yield strength at $r = a$. Substituting $r = a$ into equation (1) allows us to rewrite equation (1) as:

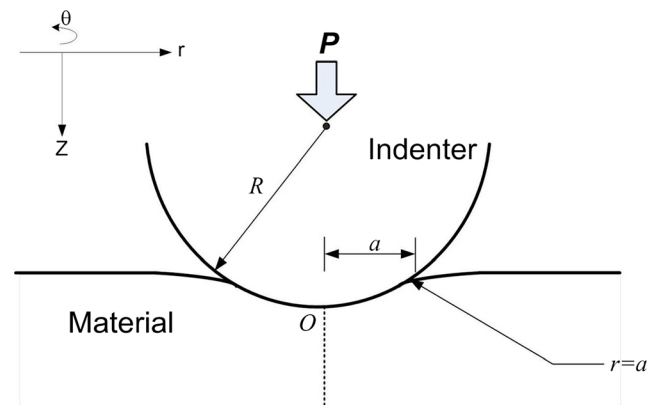$$\sigma_r = -\sigma_\theta = \frac{(1-2\nu)}{2}\cdot p_m \tag{2}$$

Fig. 1 Schematic diagram of Hertzian elastic contact: maximum tensile stress occurs at $r = a$

When $\nu = 0.3$, equation (2) is equal to equation (3) (we use a Poisson's ratio of 0.3 because this is a good approximate value for most metallic materials):

$$\sigma_r = -\sigma_\theta = 0.2 \cdot p_m \tag{3}$$

By inserting equation (3) into the von Mises yield criterion, we obtain equation (4), which is expressed in terms of the yield strength:

$$p_m^y = 2.88 \cdot \sigma_{ys} \tag{4}$$

Equation (4) indicates that when the indentation mean pressure reaches 2.88 times the yield strength of the metallic material, yielding occurs at $r = a$. We define equation (4) as the first critical condition required for crack extension in the critical stress model because at that value, ring cracking is induced in brittle materials, such as glasses and ceramics [11].The second critical condition required for crack extension can be defined by elastic-plastic contact theory. While brittle materials, such as glass and ceramic, crack without plastic deformation ahead of the crack tip, brittle metallic materials undergo plastic deformation before crack extension; thus, a small amount of plastic deformation must be considered through elastic-plastic theory. Yielding at $r = a$ means that a plastic zone is formed on the surface. Beyond that point, elastic theory no longer applies to the indentation stress field, so elastic-plastic theory is applied. To analyze the elastic-plastic stress beneath a spherical indenter, Johnson [12] proposed an extending cavity model, which was a modification of Hill's spherical cavity model. Figure 2 shows a schematic diagram of the stress field according to the extended cavity model. Johnson [12] postulated that the contact surface of the indenter is encased in a hemispherical core of radius a and that the stress state within the core is hydrostatic, p_i. He assumed that the stresses and displacement outside the core have radial

Fig. 2 Schematic diagram of the expanding cavity model

symmetry and are the same as in an infinite elastic and perfectly plastic body containing a spherical cavity under pressure p_i. He also assumed that the hydrostatic stress in the core is equal to the radial stress at the interface between the core and the plastic zone. According to Johnson's theory, within the plastic zone $a < r < c$, the stresses are given by the following equations:

$$\frac{\sigma_r}{\sigma_{ys}} = -2\ln\left(\frac{c}{r}\right) - \frac{2}{3} \tag{5}$$

$$\frac{\sigma_\theta}{\sigma_{ys}} = -2\ln\left(\frac{c}{r}\right) + \frac{1}{3} \tag{6}$$

where c is the radius of the plastic zone and r is the radial distance from the center of the contact. At the interface between the core and the plastic zone, the radial stress σ_r, given by equation (5), is equal to the core pressure p_i with a change in sign according to Johnson's assumption. The radial distance r is equal to the core radius a at that interface. Therefore, we rewrite equation (5) as:

$$\frac{p_i}{\sigma_{ys}} = -\left[\frac{\sigma_r}{\sigma_{ys}}\right]_{r=a} = \frac{2}{3} + 2ln\left(\frac{c}{a}\right) \tag{7}$$

where p_i is the core pressure and c/a is the ratio of the plastic zone radius and the core radius. As the mean pressure is applied, c/a begins to increase. When the plastic zone reaches the specimen surface, the plastic zone radius c is equal to the core radius a. At the moment, c/a is equal to 1:

$$\frac{p_i'}{\sigma_{ys}} = \frac{2}{3} + 2ln(1) \tag{8}$$

where p_i' is the core pressure at the moment that the plastic zone reaches the specimen surface. However, the portion corresponding to equation (8) is already included in the previous elastic stress field and must be excluded from the elastic-plastic indentation field analysis. By subtracting equation (8) from equation (7), we can rewrite equation (7) as follows:

$$\frac{(p_i - p_i')}{\sigma_{ys}} = \frac{\Delta p_i}{\sigma_{ys}} = \frac{2}{3} + 2ln\left(\frac{c}{a} - 1\right) \tag{9}$$

After the plastic zone reaches the surface of the specimen, c/a continues increasing as the indentation load is applied. However, after the indentation load reaches a certain value, c/a no longer increases and remains constant [12], and the strain energy reaches its maximum value. We define the core pressure at that moment as the second critical condition required for cracking because the maximum strain energy can be used as the failure criterion to predict the critical condition for the fracturing of materials [13, 14]. However, the value of c/a at that moment is unknown and must be measured to resolve
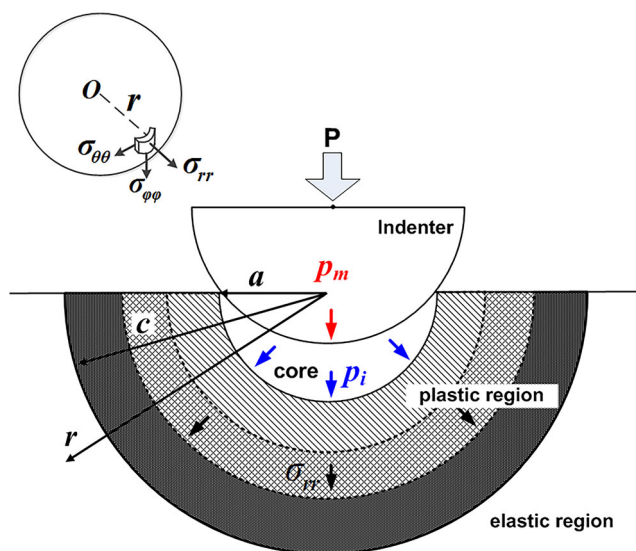
equation (9). Puttick et al. [15] investigated the relation between the indentation pressure and fracture pattern for polymethyl methacrylate (PMMA) using Hill and Johnson's spherical cavity model. They proposed a *c/a* of 2.9 for an ideal elastic-plastic material. Although the *c/a* of 2.9 was measured in PMMA, they derived the value under the condition of an elastic and perfectly plastic material, which is the same as our approach. The fracture behavior of PMMA, which is an acrylic or acrylic glass, is similar to brittle fracture [9]. Therefore, adopting a *c/a* of 2.9 in equation (9), we rewrite equation (9) as:

$$\Delta p_i = 1.95 \cdot \sigma_{ys} \tag{10}$$

Thus, we can determine the critical indentation mean pressure by summing the mean pressure in the first critical condition and the mean core pressure in the second critical condition. We can combine equation (4) and equation (10) as:

$$p_m^c = p_m^y + \Delta p_i = 4.83 \cdot \sigma_{ys} \tag{11}$$

where p_m^c is the critical mean pressure required for crack extension in the critical stress model, which depends on the yield strength of the material. The yield strength in equation (11) can be obtained by indentation testing based on an ISO technical report (ISO TR29381) [16]; the procedures for evaluating yield strength are briefly explained below.

Critical Indentation Strain Model

For brittle metallic materials, the critical mean pressure can serve as a criterion for crack extension because it occurs with little or no plastic deformation after yielding ahead of the crack tip. However, for ductile metallic materials, a large amount of plastic deformation occurs before crack extension, so plastic deformation characteristics must be considered in determining the critical point corresponding to crack extension in such metallic materials. Accordingly, we attempted to modify the critical strain model proposed by previous researchers [17] on the basis of the relation between the *J-integral* and plastic deformation characteristics, such as the plastic zone size and strain energy density, i.e., the tensile toughness. The *J-integral* has been used as a fracture parameter because of its path independence (the global and local energy release rates are equal), and it has frequently been used to describe the energy required for crack extension. A *J-integral* value that meets the size requirements and plane strain can be converted to an equivalent K_{IC}, designated K_{JC}, using equation (12) [9, 18]:

$$K_{JC} = \sqrt{\frac{J_{crit} \cdot E}{1 - \nu^2}} \tag{12}$$

where J_{crit} can be either be a J_{IC} value, measured near the initiation of ductile crack extension, or a J_C value for cleavage

fracture [9]. *E* is the elastic modulus and ν is Poisson's ratio. The *J-integral* is accumulated in the form of plastic work in the specimen during crack growth; hence, the *J-integral* is deeply related to plastic behavior and the plastic zone size and shape at the crack tip [9]. Peel and Forsyth [19] assumed that the energy release per unit crack length is balanced by the amount of plastic work performed ahead of the crack tip. The plastic work performed at the crack tip is given by:

$$W_p = 2 \cdot r_c \cdot \left(\frac{dW}{dV}\right) \tag{13}$$

where W_p is the plastic work, r_c is the critical plastic zone radius at which stable crack extension begins ahead of the crack tip, and dW/dV is the strain energy density obtained from the tensile stress-strain curve. Important parameters, such as the plastic size and plastic work which are necessary to evaluate the rate of energy release, i.e., the *J-integral*, appear in equation(13), so we adapt equation (13) to the critical strain model by assuming that $J_{IC,IIT} = W_p$, as follows:

$$J_{IC,IIT} \approx W_p = 2 \cdot r_c \cdot \left(\frac{dW}{dV}\right) \tag{14}$$

Substituting equation (14) into equation (12), we rewrite equation (12) as:

$$K_{JC} = \sqrt{\frac{2 \cdot E \cdot r_c \cdot \left(\frac{dW}{dV}\right)}{1 - \nu^2}} \tag{15}$$

The strain energy density is a tensile property that can be evaluated from the area under the tensile stress-strain curve:

$$\left(\frac{dW}{dV}\right) = \int_0^{\varepsilon_f} \sigma d\varepsilon \tag{16}$$

where ε_f is the true fracture strain determined by tensile tests. Several mathematical approximations have been suggested to estimate the strain energy density. For ductile metals with stress-strain curves similar to those of structural steel, the area under the curve can be approximated by [20]:

$$\left(\frac{dW}{dV}\right) = \frac{\sigma_{ys} + \sigma_{uts}}{2} \cdot \varepsilon_f = \sigma_R \cdot \varepsilon_f \tag{17}$$

where σ_R is the flow stress, σ_{ys} and σ_{uts} are the yield strength and ultimate tensile strength, respectively, and ε_f is the true fracture strain. Using equation (15), equation (12) can be expressed as a function of the material properties and the plastic zone radius:

$$K_{JC} = \sqrt{\frac{2 \cdot E \cdot r_c \cdot \sigma_R \cdot \varepsilon_f}{1 - \nu^2}} \tag{18}$$

Equation (18) is similar to the formula in the critical strain model proposed by Han and Rosenfield [17], except that the

characteristic length, which is the parameter associated with the microstructure, is replaced by the plastic zone size. By considering the plastic zone size, it is possible to predict the relative capacity for crack extension resistance ahead of the crack tip based on material deformability. Among the parameters in equation (18), tensile properties, such as the yield strength, tensile strength and elastic modulus can be evaluated from instrumented indentation tests based on an ISO technical report (ISO TR29381) [16]. The procedure for evaluating the tensile properties involves four steps, as illustrated in Fig. 3: step 1 – determination of the contact area, step 2 – definition of the true stress and strain, step 3 – fitting to the constitutive equation, and step 4 – evaluation of the tensile properties [16]. Partial repetition of the load-removal procedure is performed fifteen times before step 1. Three important parameters must be obtained from each partial loading-unloading curve: the maximum load, L_{max}; the maximum depth, h_{max}; and the elastic unloading stiffness, S, which is defined as the slope of the upper portion of the unloading curve during the initial stage of unloading (also called the contact stiffness), as illustrated in Fig. 3. Determination of the exact contact depth is important for determining the contact area. During spherical indentation testing, materials exhibit two types of response: elastic deflection and plastic pile-up. Oliver and Pharr [21] defined elastic deflection h_d as:

$$h_d = w\frac{L_{max}}{S} \tag{19}$$

where w is a constant that depends on the geometry of the indenter ($w = 0.75$ for a spherical indenter). We set w to 0.75. The other response is the plastic pile-up behavior [22, 23, 25], which depends on the work-hardening exponent n and h_{max}/R:

$$h_{pile} = f\left(n, \frac{h_{max}}{R}\right) \tag{20}$$

where h_{pile} is the plastic pile-up height and R is the indenter radius. From Eqs. (19) and (20), the contact depth(h_c) can be obtained as:

$$h_c = h_{max} - h_d + h_{pile} \tag{21}$$

After the contact depth is determined, the contact area, A_c, can be calculated from the relationship between the contact area and contact depth:

$$A_c = \pi\left(2Rh_c - h_c^2\right) \tag{22}$$

In step 2, the uniaxial true stress is determined from the maximum load, L_{max}, and the contact area, A_c. According to Tabor's approach [24], the mean indentation pressure has the following linear relationship with the uniaxial true stress:

$$\sigma_r = \frac{p_m}{\psi} = \frac{1}{\psi}\frac{L}{A_c} \tag{23}$$

where σ_r is the true stress obtained from the indentation, p_m is the mean indentation pressure and ψ is a plastic constraint factor. equation (23) is widely used in indentation research, and there are various definitions of the value of the plastic constraint factor ψ [24–27]. We use a plastic constraint factor of 3 to evaluate the true stress. The uniaxial true stain is determined from the geometric parameter a/R based on the deformation shape and the strain distribution under a spherical indenter [24, 25, 27]:
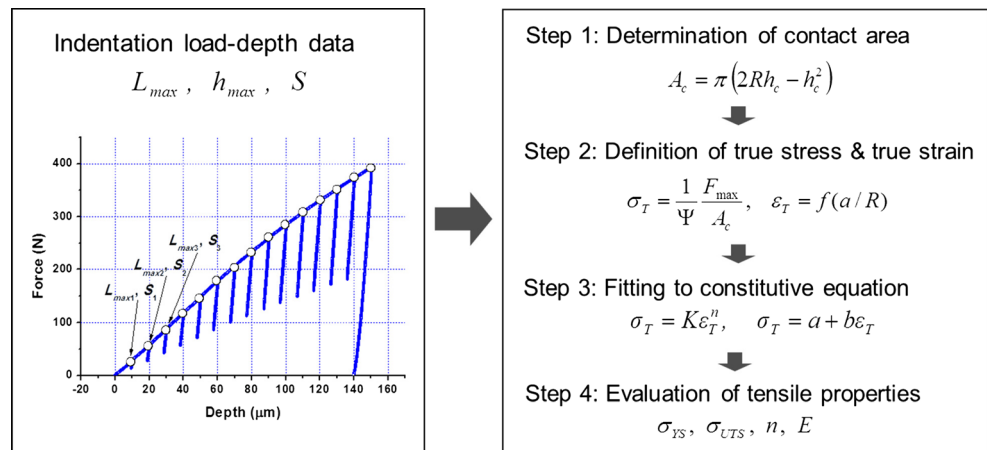
$$\varepsilon_r = f(a/R) \tag{24}$$

where a is the contact radius and R is the indenter radius. In step 3, the true stress and strain obtained by instrumented indentation testing are fitted using two constitutive equations:

$$\sigma = K\varepsilon^n \tag{25}$$

$$\sigma = A + E_T\varepsilon \tag{26}$$

Fig. 3 Schematic procedure for evaluating the tensile properties using instrumented indentation

where K is the strength coefficient, n is the strain-hardening exponent and E_T is the tangential modulus of the material. equation (25) is used for common metals that show power-law hardening, while equation (26) is used for austenitic materials, such as stainless steel, that show linear hardening. In step 4, the tensile properties are determined. The elastic modulus is measured from the indentation load-depth curve to determine the yield strength. Oliver and Pharr [21] expressed the elastic modulus as a function of contact stiffness and contact area as follows:

$$E_r = \frac{\sqrt{\pi}}{2}\frac{S}{\sqrt{A_c}} \qquad (27)$$

where E_r is the reduced elastic modulus measured from indentation, S is the contact stiffness and A_c is the contact area. The yield strength is determined as the interception of the fitted stress-strain curve and the linear curve with the slope of the elastic modulus of 0.2 offset from the origin. The strain-hardening exponent is determined from the fitting curve of the stress-strain curve. The ultimate tensile strain is the same as the strain-hardening exponent according to the theory of instability in tension [20]. The ultimate tensile strength can be determined at the ultimate tensile strain, which is obtained from the strain-hardening exponent. Finally, we can obtain the yield strength, tensile strength and elastic modulus from indentation testing. However, the other parameters in equation (17), such as the critical plastic zone r_c and the fracture strain ε_f cannot be directly obtained from the indentation load-depth curve.

The key point in this model is to assess the critical plastic zone size and the fracture strain using instrumented indentation. However, fracture does not occur in the material beneath the indenter during indentation; thus, the fracture strain in tension cannot be estimated by indentation testing. To determine these two parameters, we adopt an empirical approach for the material properties, which can be estimated by instrumented indentation. The plastic zone size can be determined by considering the balance between the plastic flow and the elastic constraint beneath the indenter. Ahead of a crack tip, the amount of plastic deformation is constrained by the surrounding material, which remains elastic. Thus, the plastic zone size depends on both the elastic and plastic properties of the material. A similar constraint occurs beneath the indenter. Therefore, if a material's elastic constraint characteristics are dominant, its plastic zone will be relatively small, but if its plastic characteristics are dominant, its plastic zone will be relatively large. This effect of the elastic and plastic characteristics with regard to the plastic zone size can be expressed as a function of the resilience, i.e., the ability of a material to absorb energy when deformed elastically. We thus attempt to derive an experimental relation between the plastic zone size and resilience. Approximate values of the plastic zone size r_c can be obtained using equation (14). In equation (14), we

measure two parameters, the J_{IC} and strain energy density, dW/dV, to calculate the r_c. The fracture toughness, J_{IC}, can be obtained by fracture toughness testing. dW/dV can be obtained by calculating the area under the tensile stress-strain curve through equation (16). Detailed procedures for fracture toughness and tensile testing are explained below. Resilience can be measured from the tensile stress-strain curve using equation (28) [20]:

$$U_r = \frac{\sigma_{ys}^2}{2E} \qquad (28)$$

where σ_{ys} is the yield strength and E is elastic modulus. The yield strength and elastic modulus can be obtained by indentation testing based on ISO TR29381 [16]. As Fig. 4 shows, an experimental relation between the plastic zone size and resilience can be derived:

$$\sqrt{r_c} = 0.10947 \cdot (U_R)^{0.3594} \qquad (29)$$

Using a similar approach, the fracture strain can be considered in terms of ductility. Ductility is the extent to which a metal can be deformed without fracture in a metalworking process and is usually determined by measuring the elongation during tensile testing. Nelson and Winlock [28] suggested that elongation can be expressed as the uniform strain to the point at which necking begins. From a ductility perspective, fracture strain is related to the uniform strain, although the uniform strain might not represent the fracture strain completely. We obtain both the fracture strain and uniform stain from tensile testing for 27 metallic materials listed in Table 1 and derive the following experimental relation between fracture strain and uniform strain, illustrated in Fig. 5:
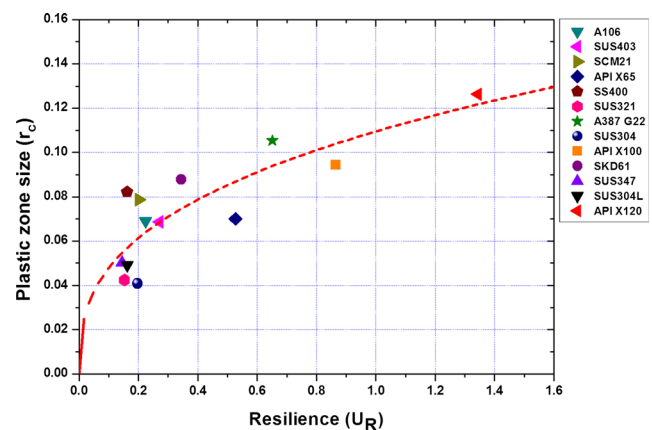
$$e_f = 0.08388 + 1.36553 \cdot \varepsilon_u \qquad (30)$$

Fig. 4 Relationship between the critical plastic zone size calculated from the fracture and tensile test results and the resilience measured by the indentation test

Table 1 Tensile properties of the tested materials

Material		E (MPa)	σ_{YS} (MPa)	σ_{UTS} (MPa)	n	e_f	ε_f
Carbon steels	SKH51	207	295	784	0.259	0.171	0.117
	A387 G11	207	555	854	0.141	0.214	0.081
	SK3	207	315	707	0.263	0.356	0.180
	SKD11	207	343	808	0.255	0.118	0.099
	SCM4	207	723	994	0.130	0.168	0.066
	SUJ2	207	404	822	0.240	0.333	0.161
	SKS3	207	435	756	0.218	0.314	0.160
	S45C	207	338	728	0.269	0.273	0.147
	A106	207	305	583	0.217	0.303	0.158
	SCM21	207	289	579	0.223	0.298	0.142
	API X65	207	467	651	0.169	0.350	0.149
	SS400	207	259	497	0.238	0.380	0.182
	A387 G22	207	519	689	0.142	0.249	0.085
	API X100	207	599	918	0.141	0.251	0.089
	SKD61	207	377	766	0.235	0.310	0.142
	API X120	207	746	1023	0.130	0.200	0.054
Stainless	SUS440	207	330	821	0.256	0.215	0.118
	SUS420J2	207	398	798	0.207	0.290	0.124
	SUS403	207	335	672	0.212	0.360	0.154
	SUS321	207	252	1040	0.373	0.724	0.471
	SUS304	207	286	1138	0.359	0.774	0.493
	SUS347	207	245	999	0.369	0.644	0.416
	SUS304L	207	259	1165	0.402	0.654	0.427
Non-ferrous alloy	Al7075	70	518	622	0.080	0.136	0.050
	Al6061	70	262	300	0.062	0.124	0.082
	Al2024	70	459	669	0.152	0.165	0.128
	InCu	120	160	481	0.328	0.483	0.371

Substituting Eqs. (29) and (30) into equation (18), we can rewrite equation (18):

$$K_{JC} = 0.10947 \cdot (U_R)^{0.3594} \cdot \sqrt{\frac{2 \cdot E \cdot \sigma_R \cdot (0.08388 + 1.36553 \cdot \varepsilon_u)}{1 - \nu^2}}$$

(31)

Experimental Details

To verify the proposed fracture toughness model, uniaxial tensile tests, fracture toughness tests, and indentation tests were performed on the materials listed in Table 1, selected on the basis of industrial requirements for fracture toughness. For example, API X-grade steels are commonly used in gas and petroleum pipelines, low-alloy Cr-Mo steels are used in power plant facilities, ASTM A106 steels are used in low-temperature pipelines and 300 series stainless steels are required for pipes in nuclear power plants. Various structural steels and tool steels are used in the fracture toughness tests.

The uniaxial tensile tests were conducted according to ASTM E8:09 [29] at room temperature. Smooth round

6 mm-diameter test specimens, proportional in size to full-size specimens, were used, and the gage length was 25 mm. The tensile tests were performed on an INSTRON 5582 material testing machine with a cross-head speed of 1 mm/min. To obtain reliable average values for the tensile properties, at
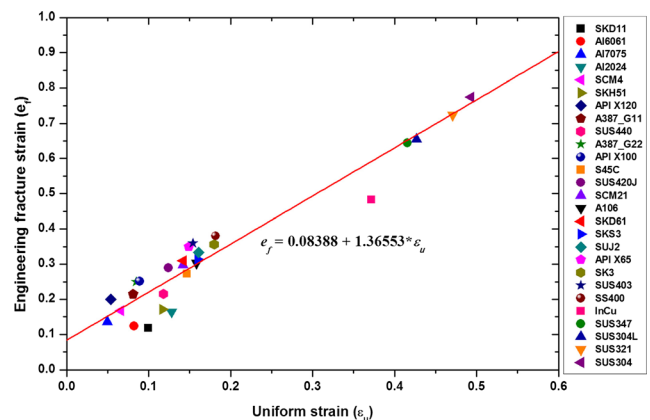
Fig. 5 Relationship between engineering fracture strain and uniform strain measured by the tensile test

least five tensile tests was conducted. The tensile properties measured by the tensile test are listed in Table 1.

Instrumented indentation tests were performed using an AIS 2100 portable indentation system (Frontics Inc., South Korea). This indentation system applies and measures real-time indentation loads and depths with a 300-kgf load cell and a linear variable displacement transducer with resolution of 0.002 kgf and 0.1 μm. The indenter was a tungsten carbide ball with a 0.25 μm radius, and testing was performed under displacement-controlled conditions at an indentation speed of 0.3 μm/min. The maximum indentation depth was 150 μm. Fifteen loading cycles, with unloading down to 50 % of the maximum load, were applied at 10 μm intervals. At least five sets of indentation data were obtained from indentation tests on each material, and the average values were used to analyze the fracture toughness. Indentation specimens were 20 × 20 × 20 mm in size, and their surfaces were polished with 1-μm Al_2O_3 powder.

The fracture toughness tests were performed according to ASTM E1820 [2] using two methods: the basic procedure and the resistance curve procedure. The basic method was used for materials that did not exhibit significant stable crack growth prior to fracture instability. The fracture toughness J_C was measured using the basic method. The resistance curve method was used to measure the fracture toughness J_{IC} near the onset of ductile crack extension, i.e., stable crack growth. A J-R curve was obtained using the single- specimen unloading compliance method: the crack length was computed at regular intervals while testing each specimen by partially unloading the specimen and measuring the compliance. The configuration of the SENB (single-edge notched bending) specimens is shown in Fig. 6, and the results of the fracture toughness test and information about the specimen thickness are summarized in Table 2.

All test specimens with an orientation corresponding to loading in the longitudinal direction and crack propagation in the transverse direction were extracted from rolled plate. Specimens were extracted from the disk and hollow orientation of L-R, i.e., loading in the longitudinal direction and crack propagation in the radial direction. Straight fatigue pre-cracks were made on the specimens in front of the side-notch to make the ratio of the total crack length to the specimen width (a/W) between 0.5 and 0.7 because the unloading compliance technique is less sensitive for
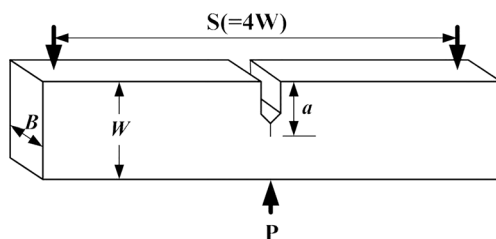
Table 2 Fracture toughness of the tested materials

Material		B	J_{Ic} or J_c	K_{Jc}	stdev.
Carbon steels	SKH51	8	14.57	59.75	4.4
	A387 G11	20	19.9	67.28	-
	SK3	8	34.76	88.86	10.8
	SKD11	8	40.52	98.37	6.8
	SCM4	8	43.68	106.16	0.3
	SUJ2	8	54.38	113.87	13.0
	SKS3	8	60.6	118.17	5.8
	S45C	15	144.61	181.32	5.1
	A106	13.5	304.56	263.03	13.6
	SCM21	15	339.98	281.37	12.0
	API X65	14	372.91	291.18	8.0
	SS400	20	423.05	310.21	0.1
	A387 G22	16	518.58	343.14	18.1
	API X100	19	548.24	352.8	19.0
	SKD61	20	571.61	360.58	3.0
	API X120	16	687.95	395.52	9.3
Stainless	SUS440	8	26.33	73.82	1.5
	SUS420J2	8	103.87	155.29	10.6
	SUS403	13	332.4	274.98	10.9
	SUS321	22	499.02	336.91	2.7
	SUS304	20	537.13	349.27	17.1
	SUS347	23	591.39	366.74	6.4
	SUS304L	20	666.29	389.21	11.0
Non-ferrous alloy	Al7075	8	17.24	36.42	3.6
	Al6061	8	21.61	40.86	2.0
	Al2024	8	48.2	64.07	7.5
	InCu	17	187.25	156.77	15.2

a/W < 0.5. The maximum load for fatigue pre-cracking was calculated from the following equation:

$$P_m = \frac{0.5Bb_0^2\sigma_R}{S} \tag{32}$$

where σ_R is the flow stress, which is typically the average of the yield strength and the ultimate tensile strength. After pre-cracking was performed, side grooves were machined into each specimen to maintain a straight crack front during the J-R curve test. The total thickness reduction was 0.2B.

An INSTRON 8503 was used as the fracture toughness testing instrument. The maximum interval of the extensometer was 10 μm. Fracture toughness values for each material were averaged from at least three tests. The tested materials were heated to measure the length of the original crack, i.e., the length of the fatigue pre-crack, and the length of the final physical crack, i.e., the extended length after testing at approximately 300 °C for 30 min. Stereographic microscopes were used to measure the crack length. Each crack length was

Fig. 6 Geometry of the SENB specimen used in the fracture test, according to ASTM E1820:09

measured at nine equally spaced points centered about the specimen centerline, as shown in Fig. 7. Provisional J_{IC} values were determined from the J-R curves, and verification of their validity was performed in accordance with the data requirements in ASTM E1820 [2].

Results and Discussion

Determination of the Fracture Toughness Using the Critical Indentation Stress Model

For the critical indentation stress model, the critical mean pressure required for crack extension is defined in equation (9). To estimate K_{JC} using the indentation, J_C must be measured. Lee et al. [8] confirmed that the degree of tri-axial stress generated by indentation with a spherical indenter is similar to that ahead of a crack tip. Thus, they proposed that the indentation energy per unit area until the critical fracture initiation point is related to the fracture energy. They defined the indentation load-depth area until the critical point as the critical indentation energy corresponding to the fracture energy. We define the indentation energy per unit contact area until the critical point obtained in equation (9) as the critical indentation

energy. We take the energy as the critical J-integral and call it $J_{C,IIT}$. The procedure for determining the fracture toughness through the critical indentation stress model is illustrated in Fig. 8. The critical indentation energy can be calculated from the indentation load-depth curve by:

$$J_{C,IIT} = \int_0^{h^*} \frac{L}{A_c} dh \tag{33}$$

where L is the applied load, A_c is the contact area and h^* is the critical indentation depth corresponding to the critical mean pressure. Figures 8, 9 and 10 show typical spherical indentation load-depth curves. Unlike the indentation loading curve with a sharp indenter, the indentation loading curves with spherical indenters are commonly linear because of the spherical geometry and work hardening in the materials. Thus, the loading part of the indentation load-depth curve can be assumed to be linear:

$$L = mh_c \tag{34}$$

A_c can be determined from equation (21). Substituting equations (22) and (34) into equation (33) yields

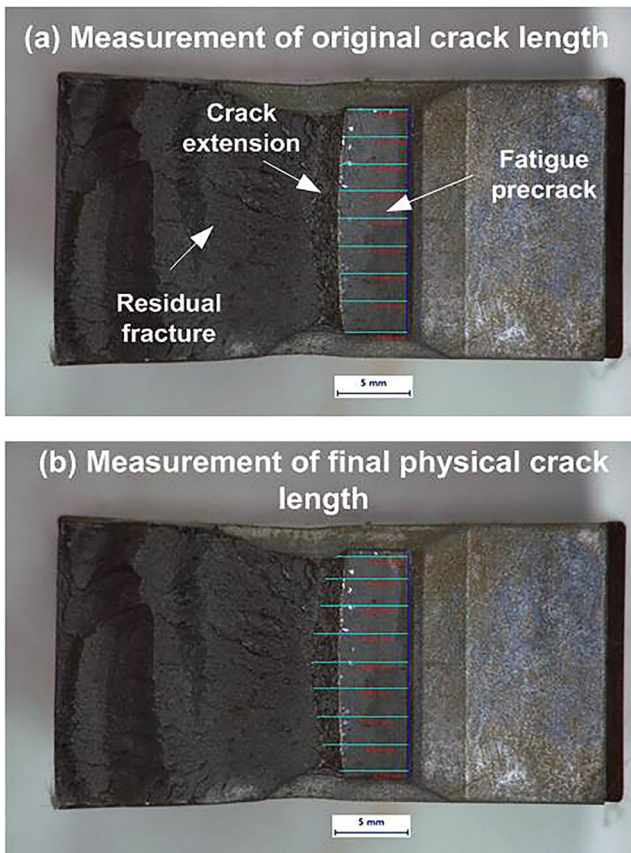$$J_{C,IIT} = \int_0^{h^*} \frac{mh_c}{\pi(2Rh_c - h_c^2)} dh \tag{35}$$

Fig. 7 Example of the optical size measurement for SCM21: (**a**) original crack length and (**b**) final physical length
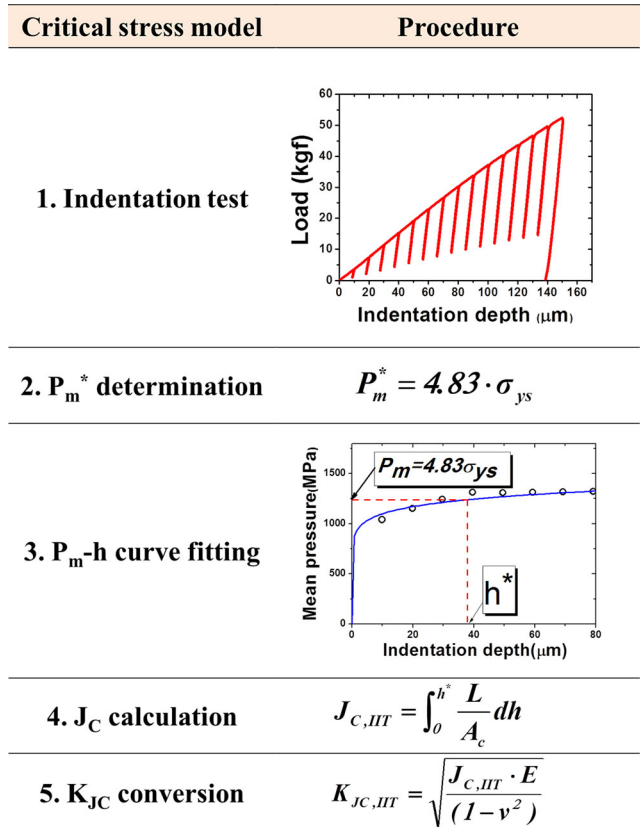

Fig. 8 Schematic procedure for determining the fracture toughness using the critical indentation stress model

Resolving equation (35) allows us to obtain equation (36).

$$J_{C,IIT} = \frac{m}{\pi}\ln\left(\frac{2R}{2R-h^*}\right) \tag{36}$$

Inserting equation (36) into equation (12) gives us

$$K_{JC} = \sqrt{\frac{E\cdot\frac{m}{\pi}\ln\left(\frac{2R}{2R-h^*}\right)}{1-v^2}} \tag{37}$$

The critical indentation depth h^* can be determined from the critical mean pressure. Figure 8 shows that the mean contact pressure at each unloading depth can be calculated from the indentation load-depth curve. The mean contact pressure points are then fitted to a constitutive equation by a simple power-law:

$$p_m = a\cdot h^b \tag{38}$$

where a and b are fitting constants. Substituting the critical mean pressure from equation (11) into equation (38) allows us to calculate the critical indentation depth, and inserting the critical indentation depth into equation (37) enables us to determine the fracture toughness of brittle metallic materials.

Determination of the Fracture Toughness Using the Critical Indentation Strain Model

Recalling equation (31), we must evaluate various inputs, such as the tensile properties, including the flow stress, resilience, elastic modulus, and uniform strain. The values of all the parameters in equation (31) can be determined by indentation testing. The procedure for determining fracture toughness through the critical indentation strain model is illustrated in Fig. 9. The strain-hardening exponent can be obtained from the fitting curve of the true stress and strain in step 4. However, the value of the strain-hardening exponent must be determined preliminarily in step 1 to calculate the contact depth. Hence the following iterative method is used to obtain the strain-hardening exponent in advance. In step 1, an imaginary strain-hardening exponent is pre-determined, and its value is compared repeatedly with the strain-hardening exponent in step 4 [16]. When the two values are the same, the value is established as the strain-hardening exponent obtained from indentation testing. However, the iteration method produces large self-deviation. Hence, we use an alternative method to determine the strain-hardening exponent. The strain- hardening exponent is a material constant that is used in calculations of stress-strain behavior during work hardening and is determined from an empirical representation over the range of plastic deformation of the true stress and strain curve. In an indentation process, the shape of the indentation loading curve reflects the hardening behavior of the indented material.

Critical strain model	Procedure
1. Indentation test	
2. Parameters Calculation	σ_{ys}, σ_{uts}, ε_u, U_R
3. Function part	$r_c = f(U_R),\ e_f = f(\varepsilon_u)$
4. J_{IC} calculation	$J_{IC,IIT} = 2\cdot f(U_R)\cdot\sigma_R\cdot f(\varepsilon_u)$
5. K_{JC} conversion	$K_{JC,IIT} = \sqrt{\dfrac{J_{IC,IIT}\cdot E}{(1-v^2)}}$
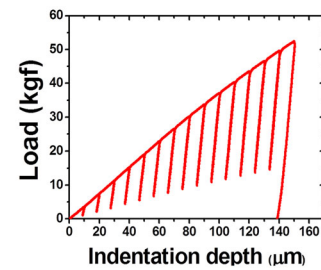
Fig. 9 Schematic procedure for determining the fracture toughness using the critical indentation strain model

The strain-hardening exponent is defined by analyzing the slope of the indentation loading curve. The slope m of the loading curve can be expressed by the indentation loads and depths at each unloading point (Fig. 10):

$$m_{ij} = \frac{L_i - L_j}{h_i - h_j} \tag{39}$$

where i and j are the number of unloadings and L and h are the indentation load and depth, respectively. The loading slopes are calculated at 10 μm intervals up to 150 μm through depth
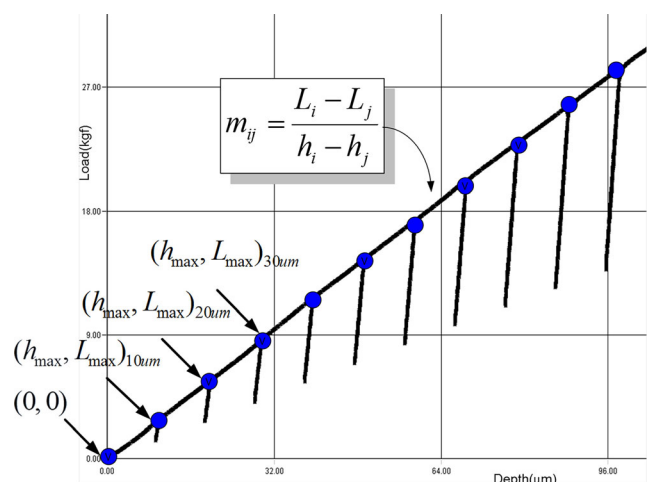

Fig. 10 Schematic diagram of the slope m of the indentation loading curve

control; then, we can obtain the slope m_{ij}. The slope ratio, p is defined as the minimum value of the slope divided by the maximum value:

$$p = \frac{m_{min}}{m_{max}} \qquad (40)$$

The relationship between p and the strain-hardening exponent n is shown in Fig. 11. The strain-hardening exponents of 27 metallic materials obtained from tensile testing are detailed in Table 1. Although large variation is observed for some materials, a good proportional relationship is observed overall. From these results, the following positive linear relation is derived to estimate the strain-hardening exponent:

$$n = -0.54033 + 1.07078 \cdot p \qquad (41)$$

The data fitting is performed by least squares regression, and the linear fitting is the most suitable with the least data deviation.

Comparison of the Fracture Toughness Measured by Indentation and Fracture Testing

The fracture toughness values obtained from equation (37) and equation (31) are compared with those from conventional fracture tests in Figs. 12 and 13, respectively. The results for brittle metallic materials, shown in Fig. 12, indicate an overall variation of approximately 15 % between the indentation and fracture tests, but the Al-alloy results show slightly larger errors than the others. This is expected because of the difference in the Poisson's ratio: a value of 0.3 was assumed for all materials, but some nonferrous metals, such as Al-alloys, have Poisson's ratios in the range 0.33–0.35. This affects the critical stress criterion in equation (37), and it is responsible for the larger error for Al-alloys in the final results. We confirmed that the accuracy of the Al-alloy results increases by approximately 3 % when a Poisson's ratio of 0.35, which is obtained from
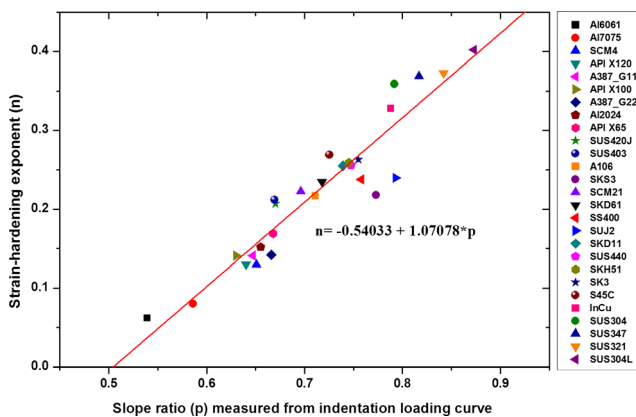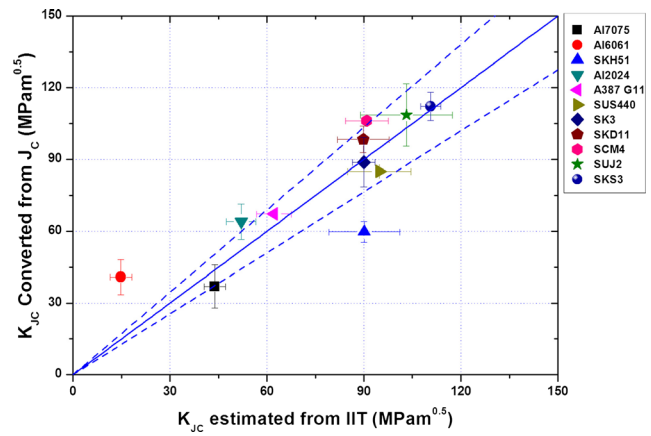

Fig. 12 Comparison of the fracture toughness in the fracture tests and indentation tests of brittle metallic materials (the dotted lines indicate a deviation of 15 %)

tensile testing, is used to estimate the fracture toughness in equation (37). However, further study is required because we cannot measure the Poisson's ratios using indentation testing: large errors occur when the unknown material to be tested is Al-alloy.

The fracture toughness values obtained for ductile materials exhibit variation of approximately 20 % between the fracture test and indentation test results as shown in Fig. 13. For most materials, the fracture toughness values obtained from indentation are lower than those obtained from fracture testing. If we consider the universal deviation in fracture toughness in the upper transition or upper shelf region [30], Fig. 13 shows mostly good agreement.

Further discussion may be required for some materials such as S45C and SUS420J2, which show larger deviations than the other materials. The final fracture of these two materials occurs under increasing load, but the fracture surface exhibits ductile tearing. Thus, they exhibit both ductile and brittle fracture characteristics. Such characteristics correspond to the fracture behavior of materials in the transition temperature
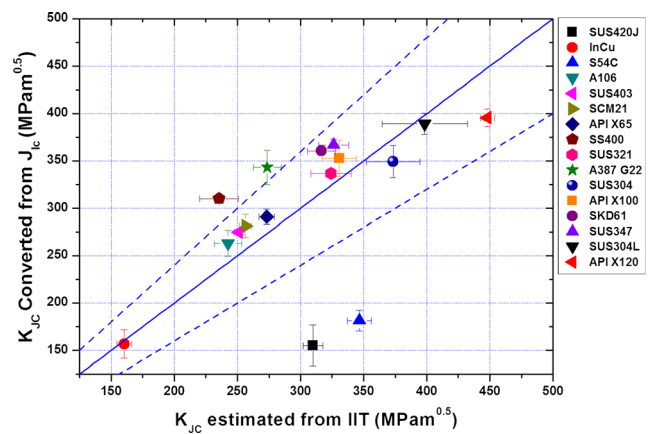

Fig. 11 Relationship between the slope ratio p evaluated from the indentation loading curve and the strain-hardening exponent measured by the tensile test

Fig. 13 Comparison of the fracture toughness in the fracture tests and indentation tests of ductile metallic materials (the dotted lines indicate a deviation of 20 %)
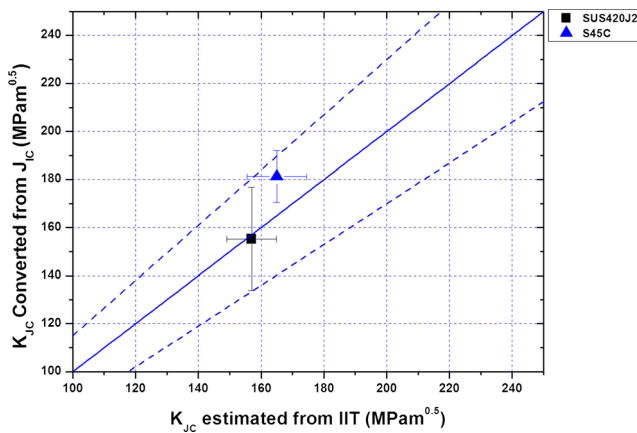
Fig. 14 Results of the fracture toughness for transition materials using the revised critical stress model (the dotted lines indicate a deviation of 15 %)

region; therefore, we define these two materials as transition materials. Given the fracture behavior of transition materials, we attempted to find an applicable modification of the critical stress model. We assumed that the fracture of transition materials is initiated when the mean contact pressure reaches the ultimate tensile strength in the tensile test. According to the Tabor relationship [24], this assumption can be expressed as:

$$p_{m,transition}^c = 3 \cdot \sigma_{uts} \tag{42}$$

where $p_{m,transition}^c$ is the indentation stress required for crack extension for transition materials and σ_{uts} is the tensile strength evaluated by indentation testing. Equation (42) refers to the modified critical stress criterion for transition materials only, and reanalyzing the results for transition materials improved the accuracy, as shown in Fig. 14. This approach may be applicable to estimation of the variation in fracture toughness in the low-temperature region. However, the criterion in equation (42) has no physical meaning, and further study is required. In addition, issues involved in distinguishing the types of models remain. We must know preliminarily whether the tested material corresponds to the critical stress or critical strain criterion (or perhaps the modified critical stress criterion) to apply the proposed model. When a material to be tested is unknown or the fracture toughness of the material is altered due to embrittlement induced by degradation or low temperature, we need a method or procedure for selection one of the models. This issue will be discussed in future work.

Conclusion

We propose a new model for estimating the fracture toughness of metallic materials using instrumented indentation testing with a spherical indenter. The model has two forms: a critical indentation stress model and a critical indentation strain

model. Different criteria were applied to each model to determine the critical fracture point during indentation. In the critical indentation stress model, we confirmed that the critical mean pressure, derived from contact mechanics, can be used as the criterion to estimate the fracture toughness of brittle metallic materials. In the critical indentation strain model, the equation derived from the relation between the energy release rate and the plastic deformation characteristics is valid for estimating the fracture toughness of ductile metallic materials. Uniaxial tensile tests, fracture toughness tests and instrumented indentation tests were performed on 27 materials to verify the proposed fracture toughness models. The results show mostly good agreement between the K_{JC} values obtained from the indentation tests and those obtained from standard fracture toughness tests.

References

1. ASTM standard E399 (2009) Standard test method for linear-elastic plan-strain fracture toughness K_IC of metallic materials, ASTM. doi: 10.1520/E0399-09
2. ASTM Standard E1820 (2009) Standard test method for measurement of fracture toughness, ASTM. doi: 10.1520/E1820-09
3. British Standard 7448-1 (1991) Fracture mechanics toughness tests, The British Standards Institution
4. Lawn BR, Wilshaw R (1975) Indentation fracture: principles and applications. J Mater Sci 10(6):1049–1081. doi:10.1007/BF00823224
5. Ju JB (2003) Investigations of fracture characteristics of natural gas pipeline weldment through the modeling of metallurgical and mechanical factors. Dissertation, Seoul National University
6. Byun TS, Kim JW, Hong JH (1998) A theoretical model for determination of fracture toughness of reactor pressure vessel steels in the transition region from automated ball indentation test. J Nucl Mater 252(3):187–194. doi:10.1016/S0022-3115(97)00338-3
7. Haggag FM, Nanstad RK, Braski DN (1989) Structural integrity evaluation based on an innovative field indentation microprobe. ASME PVP 170:101–107
8. Lee JS, Jang JI, Lee BW et al (2006) An instrumented indentation technique for estimating fracture toughness of ductile materials: a critical indentation energy model based on continuum damage mechanics. Acta Mater 54(4):1101–1109. doi:10.1016/j.actamat.2005.10.033
9. Anderson TL (1994) Fracture mechanics: fundamentals and application, 2nd edn. CRC press, London
10. Hertz H (1881) On the contact of elastic solids. J Reine Angew Math 92:156–171
11. Frank FC, Lawn BR (1967) On the theory of Hertzian fracture. Proc R Soc London A 299:291–306
12. Johnson KL (1985) Contact mechanics. Cambridge University Press, London
13. Li QM (2001) Strain energy density failure criterion. Int J Solids Struct 38(38–39):6997–7013. doi:10.1016/S0020-7683(01)00005-1
14. Qu RT et al (2016) Generalized energy failure criterion. Scientific Reports 6: Article 23359. doi:10.1038/srep23359

15. Puttick KE (1978) Indentation fracture of oriented polymethylmethacrylate. J Phys D Appl Phys 11:L69–L71. doi:10.1088/0022-3727/11/4/022

16. ISO/TR 29381 (2008) Measurement of mechanical properties by an instrumented indentation test – indentation tensile properties. International Organization for Standardization (ISO)

17. Hahn GT, Rosenfield AR (1968) Sources of fracture toughness: the relation between K_{Ic} and the ordinary tensile properties of metals. ASTM STP 432:5–32. doi:10.1520/STP33617S

18. Barsom JM, Rolfe ST (1999) Fracture and fatigue control in structure: applications of fracture mechanics, Third edition. ASTM

19. Peel CJ, Forsyth PJE (1973) The effect of composition changes on the fracture toughness of an Al-Zn-Mg-Cu-Mn forging alloy. Metal Sci J 7(1):121–127. doi:10.1179/030634573790445622

20. Dieter GE (1988) Mechanical metallurgy. McGraw-Hill, New York

21. Oliver WC, Pharr GM (1992) An improved technique for determining hardness and elastic modulus using load and displacement sensing indentation experiments. J Mater Res 7(6):1564–1583. doi:10.1557/JMR.1992.1564

22. Kim JY, Lee KW, Lee SK, Kwon D (2006) Determination of tensile properties by instrumented indentation technique: representative stress and strain approach. Surf Coat Tech 201(7):4278–4283. doi:10.1016/j.surfcoat.2006.08.054

23. Kim SH, Lee BW, Choi Y, Kwon D (2006) Quantitative determination of contact depth during spherical indentation of metallic materials—a FEM study. Mater Sci Eng A 415(1–2):59–65. doi:10.1016/j.msea.2005.08.217

24. Tabor D (1951) The hardness of metals. Clarendon, Oxford

25. Ahn JH, Kwon D (2001) Derivation of plastic stress-strain relationship from ball indentations: examination of strain definition and pileup effect. J Mater Res 16(11):3170–3178. doi:10.1557/JMR.2001.0437

26. Sundararajan G, Tirupataiah Y (2006) The localization of plastic flow under dynamic indentation conditions: I. experimental results. Acta Mater 54(3):565–575. doi:10.1016/j.actamat.2005.09.022

27. Kang SK, Kim YC, Kim KH, Kim JY, Kwon D (2013) Extended expanding cavity model for measurement of flow properties using instrumented spherical indentation. Int J Plastic 49:1–15. doi:10.1016/j.ijplas.2013.02.014

28. Nelson PG, Winlock J (1949) Strength of materials. ASTM Bull 156:53

29. ASTM standard E8 (2009) Standard test methods for tension testing of metallic materials, ASTM. doi: 10.1520/E0008_E0008M-09

30. Iwadate T, Tanaka Y, Ono S, Watanabe J (1983) An analysis of elastic-plastic fracture toughness behavior for J_{IC} measurement in the transition region. ASTM STP 803:531–561. doi:10.1520/STP36785S